

Formation of primordial supermassive stars by burst accretion

Y. Sakurai¹, T. Hosokawa², N. Yoshida³, and H. W. Yorke⁴

¹*Department of Physics, The University of Tokyo, Tokyo 113-0033, Japan*

²*Department of Physics and Research Center for the Early Universe, The University of Tokyo, Tokyo 113-0033, Japan*

³*Kavli Institute for the Physics and Mathematics of the Universe (WPI), The University of Tokyo, Kashiwa, Chiba 277-8583, Japan*

⁴*Jet Propulsion Laboratory, California Institute of Technology, Pasadena CA 91109, USA*

Draft version 18 May 2015

ABSTRACT

Recent observations show that supermassive black holes (SMBHs) with $\sim 10^9 M_\odot$ exist at redshift $z \gtrsim 6$; how they form has yet to be explained. A promising formation channel is the so-called direct collapse model, which posits that a massive seed BH forms through gravitational collapse of a $\sim 10^5 M_\odot$ supermassive star. We study the evolution of such a supermassive star growing by rapid mass accretion. The internal stellar structure is also followed consistently in our calculation. In particular, we examine the impact of time-dependent mass accretion of repeating burst and quiescent phases that are expected to occur with a self-gravitating circumstellar disk. We show that the stellar evolution with such episodic accretion differs qualitatively from that expected with a constant accretion rate, even if the mean accretion rate is the same. Unlike the case of constant mass accretion, whereby the star expands roughly following $R_* \simeq 2.6 \times 10^3 R_\odot (M_*/100 M_\odot)^{1/2}$, the protostar can substantially contract during the quiescent phases between accretion bursts. The stellar effective temperature and ionizing photon emissivity increase accordingly as the star contracts, which can cause strong ionizing feedback and halt the mass accretion onto the star. With a fixed duration of the quiescent phase Δt_q , such contraction occurs in early evolutionary phases, i.e. for $M_* \lesssim 10^3 M_\odot$ with $\Delta t_q \simeq 10^3$ yr. For later epochs and larger masses but the same Δt_q , contraction is negligible even during quiescent phases. With larger quiescent times Δt_q , however, the star continues to contract during quiescent phases even for the higher stellar masses. We show that such behavior is well understood by comparing the interval time and the thermal relaxation time for a bloated surface layer. We conclude that the UV radiative feedback becomes effective if the quiescent phase associated by the burst accretion is longer than $\sim 10^3$ yr, which is possible in an accretion disk forming in the direct collapse model.

Key words: cosmology: theory, early Universe, stars: formation, galaxies: formation, quasars: supermassive black holes

1 INTRODUCTION

Recent observations have revealed the existence of supermassive black holes (SMBHs) with masses of $\sim 10^9 M_\odot$ at $z \gtrsim 6$ (e.g., Wu et al. 2015; Marziani & Sulentic 2012; Mortlock et al. 2011). The origin and the rapid growth of the early SMBHs remain to be elucidated.

Possible seeds of the SMBHs are remnant BHs of Population III stars with $M_{\text{BH}} \sim 100 M_\odot$ (e.g., Madau & Rees 2001; Schneider et al. 2002). Although such a $\sim 100 M_\odot$ seed BH can just barely attain a mass of $\sim 10^9 M_\odot$ by the epoch of $z \simeq 6$, by accreting material at the Eddington rate, recent studies suggest difficulties in this model. For in-

stance, radiative feedback from a BH accretion disk easily suppresses the gas supply from the intergalactic medium, so that the accretion rates fall far below the Eddington values (e.g., Alvarez, Wise & Abel 2009; Jeon et al. 2012). The BH growth time then becomes much longer than the age of the universe at $z \sim 6$,

An alternative model which circumvents these difficulties is the so-called direct collapse model. The model assumes that SMBHs are built from larger seed BHs with $M_{\text{BH}} \sim 10^5 M_\odot$ that are formed directly by gravitational collapse of supermassive stars (SMSs) of similar masses (e.g., Bromm & Loeb 2003). The BH growth time is significantly shortened in this case; a $\sim 10^5 M_\odot$ seed BH can easily grow

to become a $\sim 10^9 M_\odot$ SMBH by accretion at the Eddington rate. At reduced accretion rates, e.g. due to radiative feedback from a BH-disk system, a $\sim 10^9 M_\odot$ SMBH can still form at $z \simeq 6$ if the mean accretion rate is higher than about 50 % of \dot{M}_{Edd} . Indeed, cosmological simulations show that this is possible with efficient cold accretion flows realized in the epoch of the first-galaxy formation (e.g., Di Matteo et al. 2012).

A crucial assumption in the direct collapse model is that sufficiently massive stars are formed in a gas cloud. SMSs are supposed to form in so-called atomic-cooling haloes with $T_{\text{vir}} \sim 10^4$ K (e.g., Inayoshi & Omukai 2012; Agarwal et al. 2014; Visbal, Haiman & Bryan 2014). If molecular hydrogen cooling is inhibited in these massive primordial haloes by strong ultra-violet radiation, a gas cloud gravitationally collapses via atomic hydrogen cooling nearly isothermally at $T \simeq 8000$ K (e.g., Omukai 2001). An embryo protostar eventually forms and begins to grow via gas accretion from a surrounding envelope (e.g., Inayoshi, Omukai & Tasker 2014; Van Borm et al. 2014), analogous to normal Population III star formation (Yoshida, Omukai & Hernquist 2008). The accretion rate at this stage has the well-known temperature dependence

$$\dot{M}_* \sim \frac{c_s^{3/2}}{G} \sim 0.2 \left(\frac{T_{\text{vir}}}{10^4} \right)^{3/2} M_\odot \text{ yr}^{-1}, \quad (1)$$

where c_s is the sound speed and G is the gravitational constant. Because of the higher gas temperature during the collapse stage, the accretion rate is much higher than that for normal Pop III cases. If such rapid mass accretion continues for ~ 1 Myr, which is the lifetime of massive stars, SMSs with $10^5 - 10^6 M_\odot$ can form and ultimately provide massive BH seeds after their deaths.

A possible obstacle for the growth of SMSs via rapid mass accretion is strong radiative feedback from the central massive protostar. Even when a normal Pop III star with $\sim 100 M_\odot$ forms by accretion, stellar UV radiation becomes so strong to create an HII region that dynamically expands through the accretion envelope (e.g. McKee & Tan 2008). The gas accretion is then halted; the final stellar mass is effectively determined by this mechanism (Hosokawa et al. 2011; Hirano et al. 2014). For the case of SMS formation considered here, similar, or even stronger UV feedback might significantly reduce or even halt the gas mass accretion. This could occur because a SMS should emit copious amounts of photons; the stellar luminosity is nearly at the Eddington value, which for massive stars is proportional to stellar mass. The resulting UV feedback could thus be much stronger than for normal Pop III cases.

The strength of the stellar radiative feedback depends critically on the ionizing photon emissivity of primordial protostars, which is determined by their evolution while accreting. For normal Pop III cases with mean accretion rates of a few $\times 10^{-3} M_\odot \text{ yr}^{-1}$, an accreting protostar has a large radius during the early evolution but eventually contracts to the zero-age main-sequence (ZAMS) for $M_* \sim 100 M_\odot$ (e.g., Omukai & Palla 2003). When the protostar contracts, its ionizing photon emissivity increases and UV radiative feedback becomes effective.

By contrast, the protostellar evolution should qualitatively differ from the above at very rapid accretion rates $\dot{M}_* \gtrsim \dot{M}_{*,\text{cr}} = 4 \times 10^{-2} M_\odot \text{ yr}^{-1}$ expected in the direct col-

lapse model. In this case, a protostar continues to expand and does not contract even after the stellar mass greatly exceeds $100 M_\odot$ (Hosokawa, Omukai & Yorke 2012). The stellar radius reaches $\sim 10^4 R_\odot$ for $M_* \gtrsim 10^3 M_\odot$ (Hosokawa et al. 2013; Schleicher et al. 2013). Such a “supergiant protostar” has a low effective temperature of $T_{\text{eff}} \simeq 5000$ K and the ionizing photon emissivity for $M_* \lesssim 10^4 M_\odot$ is only $\lesssim 10^{45} \text{ s}^{-1}$, several orders of magnitude lower than for main-sequence SMSs. The resulting UV feedback should be too weak to halt the mass accretion. The rapid mass accretion should thus continue, so that SMSs finally form.

The previous studies consider only constant accretion rates. In more realistic situations, however, the mass accretion onto a growing SMS should be dynamic with highly time-dependent accretion histories. For normal Pop III cases, for instance, an accretion disk formed around a protostar becomes gravitationally unstable and fragments (e.g., Stacy, Greif & Bromm 2010; Greif et al. 2011). When such fragments migrate inward in the disk and accrete onto the star (e.g., Greif et al. 2012), the accretion rate drastically increases causing so-called “burst accretion” (e.g., Vorobyov, DeSouza & Basu 2013). In this case, the accretion history is roughly divided into two phases: the burst phases with $\dot{M}_* \sim 0.1 M_\odot \text{ yr}^{-1}$ and quiescent phases with $\dot{M}_* \sim 10^{-4} M_\odot \text{ yr}^{-1}$, whose durations are $\lesssim 10^2$ yr and $\sim 10^3 - 10^4$ yr. Such episodic accretion is also expected to occur in the direct collapse model (e.g., Inayoshi & Haiman 2014). Indeed, recent high-resolution numerical simulations report signatures of the disk fragmentation in atomic-cooling haloes (Regan, Johansson & Haehnelt 2014; Becerra et al. 2015).

In this paper, we study the evolution of SMSs with time-dependent accretion histories in which a number of accretion bursts occur. Whereas the radiative feedback is generally weak for constant accretion, a time-dependent accretion rate might significantly affect the protostellar evolution and hence the feedback strength. In quiescent phases between the bursts, for instance, accretion rates should fall below the critical rate $\dot{M}_{*,\text{cr}} = 4 \times 10^{-2} M_\odot \text{ yr}^{-1}$, above which a protostar enters the supergiant stage. The protostar may contract in this case, so that the effective temperature rises and radiative feedback becomes effective. Here, we show that, by solving the stellar interior structure numerically, this should occur even with a mean accretion rate of $\sim 0.1 M_\odot \text{ yr}^{-1}$, if the quiescent phase lasts for periods $\gtrsim 10^3$ yr.

The remainder of this paper is organized as follows. In Section 2 our numerical methods and modeling of the burst accretion are explained. The numerical results are presented in Section 3, where we also compare the protostellar evolution for constant accretion rates to the evolution for time-dependent rates with a number of accretion bursts. We discuss implications of these results in Section 4 and summarize our conclusions in Section 5.

2 NUMERICAL METHOD AND MODELING OF BURST ACCRETION

2.1 Numerical method

To calculate the stellar evolution, we use the numerical code originally developed by Yorke & Bodenheimer (2008) with

additional improvements as in Hosokawa et al. (2013). The code solves the following four basic equations of the stellar evolution:

$$\frac{\partial r}{\partial m} = \frac{1}{4\pi r^2 \rho}, \quad (2)$$

$$\frac{\partial P}{\partial m} = -\frac{Gm}{4\pi r^4}, \quad (3)$$

$$\frac{\partial l}{\partial m} = E_{\text{nuc}} - c_P \frac{\partial T}{\partial t} + \frac{\delta}{\rho} \frac{\partial P}{\partial t} \quad (4)$$

$$\frac{\partial T}{\partial m} = -\frac{GmT}{4\pi r^4 P} \nabla, \quad (5)$$

where m is the mass coordinate, r the radial distance from the center, P the total (radiation plus gas) pressure, l the local luminosity, T the temperature, ρ the density, E_{nuc} the net energy generation rate by nuclear fusion, c_P the isobaric specific heat, $\nabla \equiv \partial \ln T / \partial \ln P$ the actual temperature gradient, and $\delta \equiv -(\partial \ln \rho / \partial \ln T)_P$. The temperature gradient ∇ is evaluated in the context of mixing-length theory for convective layers. The nuclear reactions of hydrogen and helium burning are included in the code.

In Eq. (3), hydrostatic equilibrium is always assumed and the inertial term is omitted. This assumption is well-founded, because the local free-fall time in the stellar interior is generally much shorter than 10 years, the typical timescale over which the mass accretion rate varies (also see Sec. 2.2 below). Note that we consider the time-derivative in Eq. (4). Thus, thermal equilibrium is *not* assumed in our calculations.

Mass accretion is implemented by adding a mass $\dot{M}_* \Delta t$ at each time step to the outermost layer of stellar models. We assume that the newly accreting gas has the same physical quantities as in the stellar atmosphere. This will be realized if the accreting materials have enough time to adjust their thermal states to those in the atmosphere, e.g., when slowly approaching the stellar surface orbiting in a circumstellar disk. This is obviously a limiting case, and the accreting gas may have some additional thermal energy. We model this potential difference using a free-parameter η , which is the fraction of the energy advected into the star with the accreting gas to the released gravitational energy,

$$\eta \equiv \frac{L_{*,\text{acc}}}{L_{\text{acc}}} = L_{*,\text{acc}} \left(\frac{GM_* \dot{M}_*}{R_*} \right)^{-1}, \quad (6)$$

where $L_{*,\text{acc}}$ is the additional energy input to the star. The values of η adopted in our set of models are summarized in Table 1 (also see Section 2.2). As explained in Hosokawa et al. (2013), however, η actually has little effect on the stellar evolution except during early stages when $M_* \lesssim 100 M_\odot$.

We follow the growth of a primordial supermassive protostar by numerically solving the stellar structure equations. We consider several models of accreting protostars that grow via episodic accretion (see 2.2 below). Our calculations begin with an initial pre-main sequence stellar model of mass $2 M_\odot$ and radius $25 R_\odot$, whereby the initial interior structure is determined by solving the Lane-Emden equation with a polytropic index $n = 1.5$. We assume that the initial model and newly accreting gas have the primordial composition with $X = 0.72$ and $Y = 0.28$.

2.2 Modeling of burst accretion

We model accretion histories expected in the case of a self-gravitating accretion disk. Numerical simulations show that, in such cases, the accretion rate sometimes sharply increases like a burst. For instance, such a burst occurs when a fragment formed via the gravitational instability migrates inward through the disk to be accreted onto the star (Vorobyov, DeSouza & Basu 2013). Normally, such a burst is followed by a quiescent phase, when the mass accretion almost ceases. Another accretion burst can be triggered when the disk self-gravity is effective again due to mass growth of the disk from a surrounding envelope. We study the effect of burst accretion for the case of the direct collapse model.

We model accretion histories with periodic accretion bursts (e.g., Baraffe, Chabrier & Gallardo 2009; Hosokawa, Offner & Krumholz 2011), by assuming alternating constant high and low accretion rates for the burst and quiescent phases, respectively: $\dot{M}_{*,\text{b}}$ and $\dot{M}_{*,\text{q}}$. The durations of these phases are parametrized with Δt_{b} and Δt_{q} . We also assume that the transition from a burst to a quiescent phase takes place over a finite duration Δt_{t} . The accretion rates during the transition phases are given by linear interpolation. In total, we have five parameters that characterize a model accretion history: $\dot{M}_{*,\text{b}}$, $\dot{M}_{*,\text{q}}$, Δt_{b} , Δt_{q} , and Δt_{t} .

We examine four different cases with different sets of these parameters as listed in Table 1. The values are chosen so that the mean accretion rate is $0.1 M_\odot/\text{yr}$, which is expected for the direct collapse model. We compare the results of the four cases with effectively the same mean accretion rate. We start the evolutionary calculations with an accretion burst.

The finite transition phase is needed for numerical stability when calculating stellar evolution with highly time-dependent mass accretion histories. We assume finite transition phases with $\Delta t_{\text{b}} \lesssim \Delta t_{\text{t}} < \Delta t_{\text{q}}$ (see Table 1 for the adopted values). We have checked that varying the transition time by a factor of a few has little effect on the results.

3 RESULTS

3.1 Evolution with constant accretion rates

3.1.1 Normal Pop III case with $10^{-3} M_\odot \text{ yr}^{-1}$

Before presenting the protostellar evolution with the burst accretion, we briefly describe the fiducial case with a constant accretion rate for comparison. In the typical case with the accretion rate of $10^{-3} M_\odot \text{ yr}^{-1}$, a protostar goes through several distinct evolutionary stages. Let us consider the following two timescales (e.g., Stahler, Palla & Salpeter 1986; Omukai & Palla 2003; Hosokawa & Omukai 2009): the Kelvin-Helmholtz (KH) time

$$t_{\text{KH}} = \frac{GM_*^2}{R_* L_*}, \quad (7)$$

which is the thermal relaxation time over which the gravitational energy is released by radiation, and the accretion time

$$t_{\text{acc}} = \frac{M_*}{\dot{M}_*}, \quad (8)$$

Table 1. Models of episodic accretion whose mean accretion rates are about $0.1 M_{\odot}/\text{yr}$.

Model	A	B	C	D
Duration of the burst phase Δt_b [yr]	25	50	100	500
Duration of the quiescent phase Δt_q [yr]	270	540	1080	5400
Accretion rate in the burst phase $\dot{M}_{*,b}$ [M_{\odot}/yr]	1	1	1	1
Accretion rate in the quiescent phase $\dot{M}_{*,q}$ [M_{\odot}/yr]	10^{-3}	10^{-3}	10^{-3}	10^{-3}
Transition time Δt_t [yr]	50	100	200	1000
Radiative efficiency η	0.1	0.1	0.1	0.01

which is the characteristic stellar growth time. In the earliest phase when $M_* \lesssim 5 M_{\odot}$, the star evolves adiabatically, satisfying $t_{\text{acc}} < t_{\text{KH}}$. As the stellar luminosity L_* increases with increasing stellar mass, the KH time becomes shorter. The luminosity increases because the stellar interior opacity decreases according to Kramer's law ($\kappa \propto \rho T^{-3.5}$) when the temperature increases. As the opacity decreases, the heat accumulated in the interior gradually escapes outward by radiative heat transport. The timescale balance is finally inverted and the protostar begins to contract radiating the energy away from the surface. The KH contraction stage begins when $M_* \gtrsim 8 M_{\odot}$ in the case of $\dot{M} = 10^{-3} M_{\odot} \text{ yr}^{-1}$, as can be seen in Figure 1. The stellar interior temperature rises during the KH contraction stage, and finally hydrogen burning begins at the center when $M_* \simeq 40 M_{\odot}$. After this point, the evolution of the stellar radius closely traces the mass-radius relation of a ZAMS star.

Figure 1 shows that the rapid rise of the stellar ionizing photon emissivity is synchronous with the KH contraction. Before KH contraction begins, the ionizing photon emissivity is only $\sim 10^{37} \text{ sec}^{-1}$. As the star contracts and the effective temperature rises, however, the emissivity quickly reaches $\gtrsim 10^{49} \text{ sec}^{-1}$. Radiation hydrodynamic simulations show that the stellar radiation feedback operates in the late KH stage and eventually shuts off the mass accretion onto the star (e.g., Hosokawa et al. 2011).

3.1.2 Direct collapse case with $0.1 M_{\odot} \text{ yr}^{-1}$

Here, we consider protostellar evolution at the high constant accretion rate of $0.1 M_{\odot} \text{ yr}^{-1}$. Unlike the case for $10^{-3} M_{\odot} \text{ yr}^{-1}$, the protostar does not evolve to the KH contraction stage (see the dashed lines in Fig. 1). The star instead continues to expand nearly monotonically with increasing mass.

The timescale inversion described in Section 3.1.1 occurs at $M_* \simeq 22 M_{\odot}$ ($t \simeq 200 \text{ yr}$) in this case (Fig. 2). The star evolves adiabatically before this epoch. Since the rapid accretion enhances the average entropy in the stellar interior, the stellar radius at a given mass is larger than for $10^{-3} M_{\odot} \text{ yr}^{-1}$.

The protostar continues expanding even when $t_{\text{KH}} < t_{\text{acc}}$; the star radiates the internal energy through the surface, which normally makes the star contract. Hosokawa, Omukai & Yorke (2012) show that most of the stellar interior actually contracts even in this bloating phase. Basically, only the newly accreted surface layer inflates by absorbing the outward heat flux coming from the contracting interior.

The mass of the bloating surface layer has a small fraction of the total stellar mass. In the surface layer, the opacity is mostly due to H^- bound-free absorption that has a very strong temperature-dependence. As a result, the stellar effective temperature is locked at a constant value $\simeq 5000 \text{ K}$ as in the case of red-giants. From relations $T_{\text{eff}} \simeq 5000 \text{ K}$ and $L_* = 4\pi R_*^2 T_{\text{eff}}^4 \simeq L_{\text{Edd}}$, we can easily show

$$R_* \simeq 2.6 \times 10^3 R_{\odot} \left(\frac{M_*}{100 M_{\odot}} \right)^{1/2}, \quad (9)$$

which explains the numerical results very well. The evolution of ionizing photon emissivity also differs from the case with $\dot{M} = 10^{-3} M_{\odot} \text{ yr}^{-1}$. Even when $M_* > 100 M_{\odot}$, the protostar still has very low ionizing photon emissivity because of the low effective temperature. The resulting stellar UV feedback is then too weak to halt the rapid mass accretion (see Section 4).

We have found that in spite of the timescale imbalance $t_{\text{KH}} < t_{\text{acc}}$, the star continues to expand. The apparent discrepancy is explained by the fact that the normal definition of t_{KH} (Eq. 7) is a global relationship and does not consider the stellar interior structure; as we discussed above, most of the stellar mass is concentrated near the center and the bloated surface layer contains only a small fraction of the stellar mass (also see Figure 2 in Hosokawa et al. 2013).

We therefore must evaluate the local KH timescale for the surface layer by considering the actual mass distribution within a star,

$$t_{\text{KH,surf}} = \frac{f \int s_{\text{rad}} T dm}{\int dl}, \quad (10)$$

where s_{rad} is the entropy of radiation and f is a dimensionless constant of $\mathcal{O}(1)$. The latter factor is introduced to represent that only a fraction f of the total entropy is carried away over the timescale. We compare the above local KH time with the local accretion timescale for the surface layer,

$$t_{\text{acc,surf}} = \frac{f \int dm}{\dot{M}_*}. \quad (11)$$

For consistency we also include the same factor f in Eq. (11). In the following, we set $f = 0.4$ as a fit to our numerical results. We take the integration range in Eqs. (10) and (11) as $0.7 M_* \leq m \leq M_*$ to cover the surface layer. We have checked that varying the lower bound does not significantly affect the main results. Figure 2 shows that the local accretion time $t_{\text{acc,surf}}$ still remains shorter than the corresponding KH time $t_{\text{KH,surf}}$ even when the global KH

timescale satisfies $t_{\text{acc}} > t_{\text{KH}}$. The star continues to expand because, with the rapid mass accretion, the gas accumulates in the surface layer faster than it can thermally relax. In other words, part of the outgoing heat flux is trapped by the accreting gas, and the inflated surface layer cannot contract.

Below we show that these two local timescales $t_{\text{acc,surf}}$ and $t_{\text{KH,surf}}$ are also useful for understanding stellar evolution for the case of burst accretion.

3.2 Evolution with burst accretion

3.2.1 Model C

We first focus on our Model C as a fiducial case for stellar evolution with burst accretion. In this case, the burst and quiescent phases have the accretion rates $\dot{M}_{*,b} = 1 M_{\odot} \text{ yr}^{-1}$ and $\dot{M}_{*,q} = 10^{-3} M_{\odot} \text{ yr}^{-1}$ for the durations of $\Delta t_b = 100 \text{ yr}$ and $\Delta t_q = 1080 \text{ yr}$ (Table 1). The protostellar evolution is shown in Figure 3, where we note substantial differences in the evolution from the case with the constant rate $0.1 M_{\odot} \text{ yr}^{-1}$. First of all, the star contracts during the quiescent phases. At $300 \lesssim t \text{ (yr)} \lesssim 1500$, for instance, the stellar radius decreases to $100 R_{\odot}$, which is more than 10 times smaller than the super-giant protostar for the case $\dot{M} = 0.1 M_{\odot} \text{ yr}^{-1}$ at the same mass. When the star contracts, the ionizing photon emissivity increases and becomes comparable to that of the corresponding ZAMS star.

Because the accretion rate in the quiescent phase is lower than the critical rate for maintaining bloating of the star, $\simeq 4 \times 10^{-2} M_{\odot} \text{ yr}^{-1}$, the star contracts as in the normal KH contraction stage. To see this, we analytically derive an equation which describes the time evolution of the radius assuming that the contraction occurs over the KH timescale,

$$\frac{R_*}{R_{\odot}} = \left(\frac{1}{R_{*,0}/R_{\odot}} + C \frac{t-t_0}{1 \text{ yr}} \frac{1}{M_*/M_{\odot}} \right)^{-1}, \quad (12)$$

where C is a parameter, and the subscript 0 represents the quantities when the contraction begins¹. Figure 3 shows the fitting curve using Eq. (12) together with our numerical result.

The protostar expands again when the next burst accretion occurs and the ionizing photon emissivity decreases accordingly. This cycle is repeated for the following two cycles of quiescent and burst phases for $2000 \lesssim t \text{ (yr)} \lesssim 5000$. As the star becomes more massive, the features of the contraction gradually diminish. The star contracts very little during quiescent phases when $t \gtrsim 5000 \text{ yr}$, i.e., after the

¹ Derivation of Eq. (12) is as follows. Assuming that the stellar radius decreases roughly exponentially with a timescale given by Eq. (7), i.e. the KH time, the time derivative of the stellar radius is

$$\frac{dR_*}{dt} \sim -\frac{R_*}{t_{\text{KH}}} = -\frac{L_* R_*^2}{GM_*^2}. \quad (13)$$

Using the fact that stellar luminosity is well approximated by the Eddington value $\propto M_*$, Eq. (13) becomes

$$\frac{dR_*}{dt} = -\text{const.} \times \frac{R_*^2}{M_*}. \quad (14)$$

Because the stellar mass is almost constant during a quiescent phase, integrating Eq. (14) gives Eq. (12).

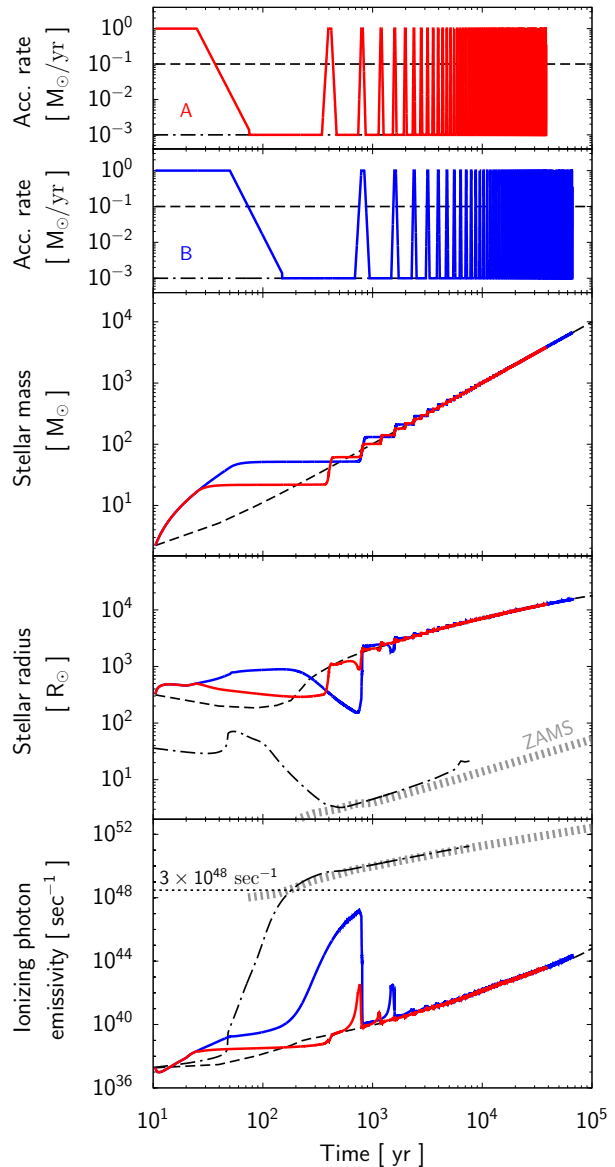


Figure 1. Time evolution of the accretion rates (top two panels), stellar mass (third panel), radius (fourth panel), and ionizing photon emissivity (bottom panel). In each panel, the red and blue lines represent Models A and B (see Table 1). The evolution with constant accretion rates of $0.1 M_{\odot} \text{ yr}^{-1}$ and $10^{-3} M_{\odot} \text{ yr}^{-1}$ are also presented with the black dashed and dotted-dashed lines respectively. In the bottom two panels, the lines for $10^{-3} M_{\odot} \text{ yr}^{-1}$ have been horizontally shifted so that the increase of stellar mass matches that for $0.1 M_{\odot} \text{ yr}^{-1}$, i.e., $M_* = 100 M_{\odot}$ at the time of 10^3 years. The radii and ionizing photon emissivity of ZAMS stars are also plotted with the thick gray dashed lines, which are also plotted assuming the same mass variation. In the bottom panel the horizontal short-dashed line represents the critical ionizing photon emissivity above which UV feedback should become effective with an accretion rate $0.1 M_{\odot} \text{ yr}^{-1}$ (see Section 4).

stellar mass exceeds $500 M_{\odot}$. Thus, UV feedback can become effective with this burst accretion model, but only for early evolutionary times.

The result is understood by comparing the duration of the quiescent phase Δt_q with the surface KH time $t_{\text{KH,surf}}$ defined in Eq. (10). For the integration range in Eq. (10),

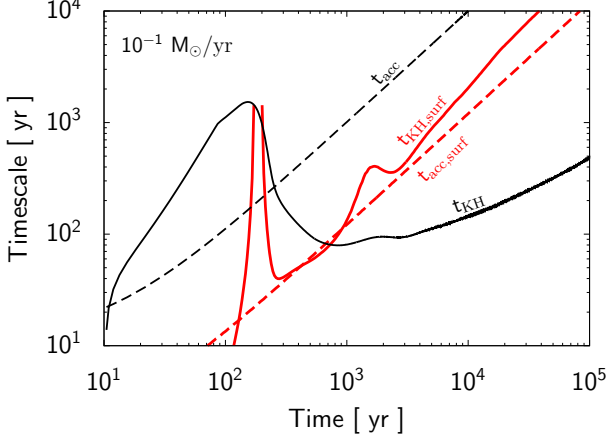


Figure 2. The evolution of timescales with the constant accretion rate of $0.1 M_{\odot} \text{ yr}^{-1}$. The black solid and dashed lines represent KH timescale t_{KH} and accretion timescale t_{acc} , respectively. The red solid and dashed lines are the local KH and accretion timescales $t_{\text{KH,surf}}$ and $t_{\text{acc,surf}}$.

we consider a layer covering $0.01 R_* \leq r \leq R_*$ that has only $\simeq 10 - 30 \%$ of the total mass but 99.9999% of the volume. As seen in Figure 4, the surface KH time monotonically increases with time (and stellar mass), except for some spiky features that appear when the protostar contracts. The mass-radius relation deviates from Eq. (9) for a brief time period. Note that Eq. (10) can also be written as

$$t_{\text{KH,surf}} \sim \frac{\int \int \frac{Gm}{r} dm}{\int dl} \propto \frac{GM_*^2}{L_* R_*} \propto M_*^{1/2}. \quad (15)$$

The first relation comes from the hydrostatic equilibrium for radiation pressure, $T_{\text{rad}} \sim P_{\text{rad}}/\rho \sim Gm/r$. The KH time increases because the stellar gravitational energy increases with mass as $\propto M_*^2/R_* \propto M_*^{3/2}$ whereas the stellar luminosity only increases as $\propto M_*$.

Figure 4 shows that, for $t \lesssim 5 \times 10^3$ yr, the surface KH time is shorter than the duration of the quiescent phases. In other words, the quiescent phase is long enough for the protostar to lose the thermal energy trapped in the surface layer. The protostar then contracts. Even in such cases, however, the stellar contraction does not immediately follow the decrease of the accretion rate. After the first burst, for instance, the accretion rate falls down \dot{M}_{cr} at $t \simeq 150$ yr (Fig. 3), but the star begins to contract only at $t \simeq 400$ yr. Figure 4 shows that the surface KH time in this epoch is really ~ 100 yr, which explains the above delay of the contraction. Figure 3 shows that this delay lengthens to $\sim 10^3$ yr after the second and third bursts, because the surface KH time increases with increasing the stellar mass as shown in Figure 4.

For $t \gtrsim 5 \times 10^3$ yr, the surface KH time is longer than the duration of the quiescent phases. The quiescent phase is now too short for the star to significantly contract and the next accretion burst begins before the stellar surface layer can appreciably relax. Consequently, the evolution of the star after this point is almost the same as in the case with the constant accretion rate $0.1 M_{\odot} \text{ yr}^{-1}$.

As discussed in Section 3.1.2, it is important to use $t_{\text{KH,surf}}$ as the thermal relaxation time for the bloated pro-

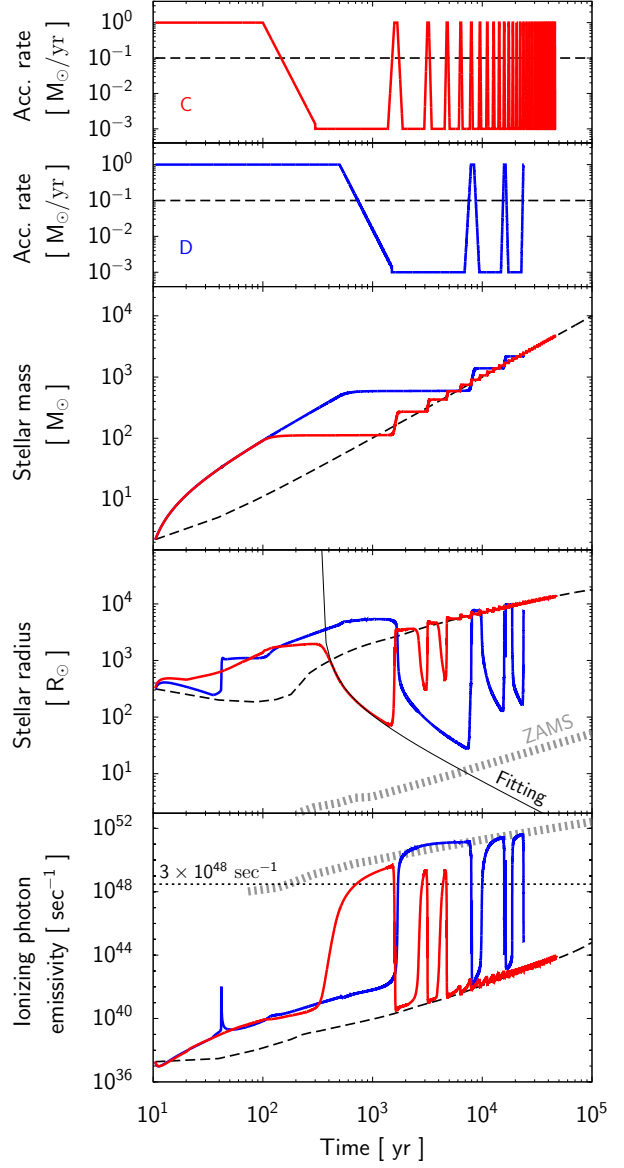


Figure 3. The same as Figure 1 but for Models C and D (red and blue lines respectively, see Table 1). In the fourth panel, the black solid line represents a fitting function of the KH contraction for Model C (see text and footnote 1).

tostars instead of the normal KH time t_{KH} since the latter does not consider the inhomogeneous density structure in the stellar interior. (see Figs. 5 and 6).

Since the normal KH time represents the thermal relaxation time for the whole star, it might appear puzzling that t_{KH} is shorter than the local surface KH time $t_{\text{KH,surf}}$ for only a part of the star. The normal KH time provides the thermal relaxation time if the following condition is satisfied:

$$\int_0^{M_*} \frac{Gm}{r} dm \sim \frac{GM_*}{R_*}, \quad (16)$$

which is not true in our case. Since most of the stellar mass is concentrated near the center as shown in Figures 5 and 6, we have

$$\int_0^{M_*} \frac{Gm}{r} dm \sim 10 - 100 \frac{GM_*}{R_*}, \quad (17)$$

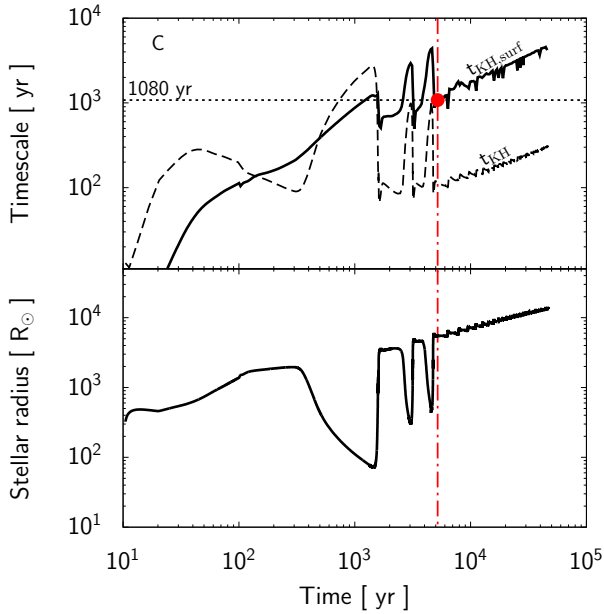


Figure 4. *Upper panel:* We compare the KH timescales with the duration of the quiescent phase Δt_q (horizontal short dashed line) in Model C. The solid and dashed lines show the time evolution of the local KH timescale for the bloated surface layer $t_{\text{KH,surf}}$ (Eq. 10) and the normal KH timescale t_{KH} (Eq. 7). *Lower panel:* the evolution of the stellar radius in Model C. The red circle in the upper panel and vertical dot-dashed line mark the point where $\Delta t_q = t_{\text{KH,surf}}$. Thus, the star can appreciably contract during quiescent phases only for earlier times.

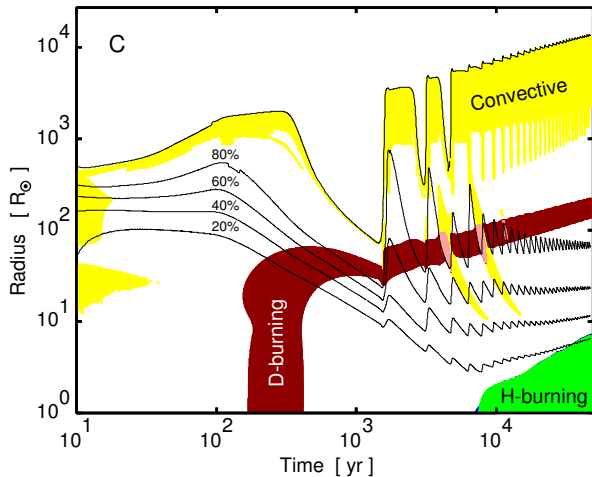


Figure 5. The evolution of the stellar interior structure in Model C. The black solid lines indicate the positions of the mass coordinates for 100% (stellar surface), 80%, 60%, 40% and 20% of the total stellar mass in descending order. The yellow regions denote layers with convection, according to mixing length theory. The brown regions show deuterium-burning layers, where the timescale over which deuterium mass fraction decreases by nuclear fusion is shorter than the main-sequence lifetime. The green region represents a hydrogen-burning convective core, which is identified measuring the depletion time for hydrogen. The pink regions are deuterium-burning convective layers. The stellar mass is roughly equal to $\bar{M}t$ for $t \gtrsim 10^3$ yr, where \bar{M} is the mean accretion rate and t is time.

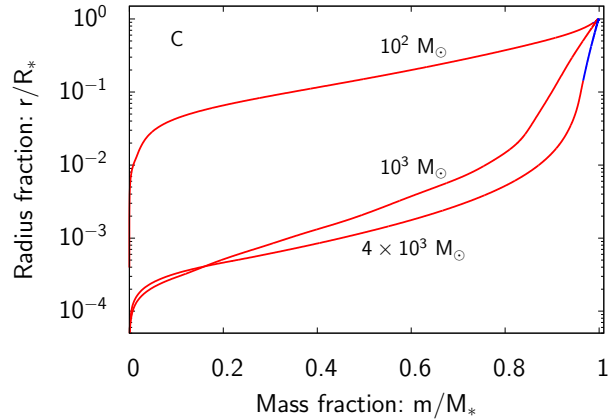


Figure 6. The mass distributions in the stellar interior in Model C. The three snapshots for $M_* = 10^2 M_\odot$ ($t = 10^2$ yr), $10^3 M_\odot$ (10^4 yr) and $4 \times 10^3 M_\odot$ (4×10^4 yr) are presented. The latter two snapshots are for the largely bloated protostars. Each profile is plotted against the normalized mass coordinate m/M_* , where m is the normal mass coordinate and M_* is the stellar mass. The vertical axis also represents the normalized radial distance from the center, r/R_* .

depending on the stellar mass and accretion history. As a result, the effective thermal relaxation time for the whole star is now $t_{\text{KH,eff}} \sim 10 - 100 \times t_{\text{KH}}$, which is always larger than the surface KH time $t_{\text{KH,surf}}$.

We confirmed that $t_{\text{KH,eff}}$ becomes comparable to Δt_q at $t \sim 1,000$ yr, which does not match the epoch when the star stops contracting. For the bloated protostar, only entropy near the stellar surface determines whether the star contracts or not. Therefore it is reasonable to use the local KH time $t_{\text{KH,surf}}$ for the surface layer only.

3.2.2 Variations with different burst accretion

We can explain the results of Models A, B, and D based on our findings for Model C. In model B, for example, the star does not significantly contract during quiescent phases for $t \gtrsim 2,000$ yr (Fig. 1). Figure 7 shows the evolution of the KH time for Model B. We see that $t_{\text{KH,surf}}$ becomes equal to the duration of the quiescent phase Δt_q at $t \simeq 2,000$ yr, which agrees with the numerical results.

Figures 1 and 3 show that, as expected, the star stops contracting earlier for quiescent phases of shorter duration. Unless the star contracts for a long time, the resulting increase of the stellar ionizing photon emissivity is not large. We conclude that the episodic accretion causes the stellar contraction and potential UV feedback only if the quiescent phase lasts for $\gtrsim 10^3$ yr.

4 DISCUSSION

4.1 UV feedback from supermassive stars evolving with burst accretion

We first discuss briefly whether UV photons from a SMS growing in mass due to burst accretion can ionize the surrounding gas to initiate strong radiative feedback. At an

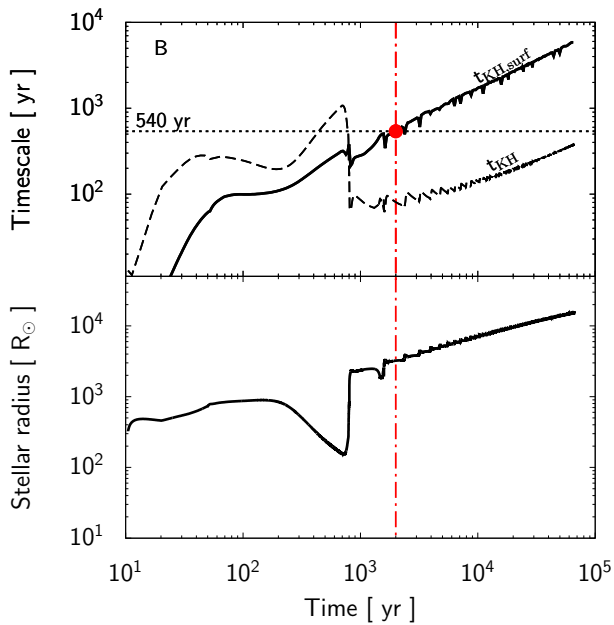


Figure 7. Same as Figure 4 but for Model B.

accretion rate $\dot{M} = 0.1 M_{\odot} \text{ yr}^{-1}$, the total number of hydrogen and helium atoms infalling per second is $3 \times 10^{48} \text{ sec}^{-1}$. Assuming that the feedback becomes effective if all the atoms are ionized, we derive an approximate lower limit of ionizing photon emissivity which induces strong feedback: $S_{\text{min}} = 3 \times 10^{48} \text{ sec}^{-1}$. This critical value is shown by the dashed horizontal lines in the bottom frames of Figures 1 and 3. In Models A and B, for which the duration of the quiescent phase Δt_q is short, the ionizing photon emissivity is always lower than S_{min} (Figure 1). By contrast, in Models C and D with the longer quiescent phase duration Δt_q , the stellar ionizing photon emissivity exceeds S_{min} when the star contracts in the quiescent phases. Radiative UV feedback becomes effective in quiescent phases when $\Delta t_q \gtrsim 10^3 \text{ yr}$, even if the mean accretion rate is $0.1 M_{\odot} \text{ yr}^{-1}$.

The above estimate provides only a necessary condition for appreciable UV feedback, because UV photons are also consumed by re-ionizing the recombining gas within an HII region. Moreover, even if an HII region appears around the star, its expansion is interrupted by the burst accretion. Suppose that the mass supply from the envelope to the disk continues after an HII region is formed. This is likely because the HII region first extends only in polar directions with respect to the disk in an early evolutionary stage (e.g., Hosokawa et al. 2011). With its mass increasing, the disk becomes gravitationally unstable, which then can cause another event of burst accretion. The stellar contraction is halted and the ionizing photon emissivity suddenly decreases as the star bloats again (see Figs. 1 and 3). As a result, the HII region quickly disappears. Some of the gas expelled by the expanding HII region might fall back onto the disk before the HII region reappears during the next stellar contraction. Thus, it is still uncertain to what extent the star can continue to grow within the context of burst accretion and intermittent UV feedback. Further studies are clearly needed to examine the overall impact of burst accretion on disk accretion and HII region formation.

4.2 Accretion histories in atomic-cooling halos

In this paper, we have modeled the time-dependent accretion histories using a simple functional form with several free parameters (Table 1). Despite progresses in 3D numerical simulations, there remains significant uncertainty in the long-term accretion history of a supermassive star. Latif et al. (2013) follow the long-term evolution in the protostellar accretion stage using the so-called sink cell technique. Their obtained accretion history shows some time-variability, but is overall rather smoother than considered in our paper. Regan, Johansson & Haehnelt (2014) and Becerra et al. (2015) use simulations with a much higher spatial resolution and find more signatures of the disk fragmentation. Although their simulations only follow the initial 10 – 100 yr in the accretion stage, the results suggest that a highly time-dependent mass accretion can be realized in the direct collapse model.

Vorobyov, DeSouza & Basu (2013) perform high resolution 2D simulations that follow the long-term evolution of a disk for normal Pop III cases. Episodic accretion occurs in these simulations with the mean accretion rate of $\sim 10^{-3} M_{\odot} \text{ yr}^{-1}$. The mean value represents the rate onto a disk from the surrounding envelope. When gas accretion occurs through a self-gravitating disk, the accretion rate onto a star becomes strongly variable. When fragmentation occurs in the disk, clumps migrate inward to the star, and the accretion rate rises up to $\sim 10^{-2} - 0.1 M_{\odot} \text{ yr}^{-1}$. In the intervals between such burst events, the accretion rate falls to $\sim 10^{-5} - 10^{-4} M_{\odot} \text{ yr}^{-1}$.

We also expect burst accretion with large variations around the mean value of $\sim 0.1 M_{\odot} \text{ yr}^{-1}$ in the direct collapse model. If the accretion rates during the quiescent phase falls to values $\dot{M}_{*,q} \lesssim 10^{-2} M_{\odot} \text{ yr}^{-1}$, the star can contract as suggested by our results.

Our calculations show that the duration of the quiescent phase is a key parameter that determines if the star contracts or not. The quiescent phase will be controlled by the following two timescales, the effective fragmentation time t_{frag} (i.e. taking into account that multiple clumps can be produced during the fragmentation process) and the migration time t_{mig} . The former is the average time for a fragment to be born in a gravitationally unstable disk or $1/(\text{rate of clump formation})$. The latter is the timescale over which the newly formed fragments migrate inward to reach the star. We expect $\Delta t_q \sim t_{\text{frag}} + t_{\text{mig}}$. If $t_{\text{frag}} < t_{\text{mig}}$, the duration of the quiescent phase will be mainly determined by t_{mig} . Conversely, if $t_{\text{frag}} > t_{\text{mig}}$, the duration is limited by t_{frag} .

Previous numerical and analytical studies give reasonable estimates for the timescales. For example, Vorobyov, Zakhochay & Dunham (2013) argue that, based on their simulations of present-day star formation, the fragmentation time should be determined by the timescale over which the disk gets mass supply from the accretion envelope,

$$t_{\text{frag}} = \frac{M_d}{\dot{M}_d}, \quad (18)$$

where M_d is the disk mass and \dot{M}_d is the infall rate onto the disk.

Inayoshi & Haiman (2014) develop an analytic model of the structure of an accretion disk around a SMS, and estimate where gravitational fragmentation occurs in the disk.

According to their model, there is a maximum radius R_f , within which the disk is unstable to fragmentation. The migration time for a fragment formed at R_f is then estimated to be

$$t_{\text{mig,max}} \simeq 4 \times 10^3 \text{ yr} \quad (19)$$

for the mean accretion rate $0.1 M_\odot \text{ yr}^{-1}$ and the central star with $M_* \lesssim 10^4 M_\odot$. This can be considered as the *maximum* timescale because a fragment formed at $R < R_f$ will have the shorter migration time, $t_{\text{mig}} < t_{\text{mig,max}}$.

We summarize the evolution of Δt_q expected from the above discussion as follows. In an early evolutionary phase for $t_{\text{frag}} < t_{\text{mig}}$, the quiescent period Δt_q is limited by the migration time t_{mig} . In this case, the quiescent phase lasts for 10^3 yr, which is the critical value for the formation of an HII region (Sec. 3.2.2), or even shorter. With the accretion rate $0.1 M_\odot \text{ yr}^{-1}$ from the envelope onto the disk, however, the fragmentation time t_{frag} exceeds the migration time when the disk mass reaches $\simeq 400 M_\odot$. After this point, the quiescent phase may become longer with increasing the stellar mass, if the disk mass is comparable to the stellar mass. Unlike in the case for constant duration Δt_q studied in the present paper, the star with high mass will further contract during prolonged quiescent phases. The stellar ionizing photon emissivity should be enhanced by this effect.

Ultimately, in order to verify the above expectation, we need to derive realistic accretion histories realized in an atomic-cooling halo. To this end, multi-dimensional hydrodynamic simulations would be necessary that follow the dynamic accretion process onto growing SMSs. Future studies combining radiation hydrodynamics simulations and stellar evolution calculations should yield more realistic models (e.g., Hosokawa et al. 2011; Smith et al. 2012; Machida & Hosokawa 2013; Kuiper & Yorke 2013; Hirano et al. 2014).

5 CONCLUSIONS

We have studied the evolution of supergiant protostars growing under episodic accretion, which is expected in a self-gravitating circumstellar disk forming in an atomic-cooling halo (e.g., Vorobyov, DeSouza & Basu 2013; Regan, Johansson & Haehnelt 2014; Inayoshi & Haiman 2014). We have followed the protostellar evolution with various assumed accretion histories of repeating short bursts and long quiescent phases. In order to examine potential impact of the burst accretion model, the adopted accretion histories have the same mean accretion rate $0.1 M_\odot \text{ yr}^{-1}$ but different variabilities (Table 1). Our findings are summarized as follows:

Burst accretion can qualitatively change the evolution of an accreting SMS. Although our previous calculations show that the stellar radius monotonically increases with increasing the mass under the constant accretion (Eq.9), this is not always the case within the framework of burst accretion; i.e. the star can contract during the quiescent phases between the bursts. During the contraction, the stellar ionizing photon emissivity greatly increases because the effective temperature rapidly rises. For a quiescent phase of length $\Delta t_q \gtrsim 10^3$ yr, the ionizing photon emissivity exceeds $3 \times 10^{48} \text{ sec}^{-1}$, which allows the formation of an HII region. As a result, UV feedback might hinder the mass accretion onto the star.

With a fixed duration of the quiescent phase Δt_q , stellar contraction can occur in an early epoch; for instance, for $M_* \lesssim 10^3 M_\odot$ with $\Delta t_q \simeq 10^3$ yr. With a longer Δt_q , however, stellar contraction will continue until the star becomes much more massive. This is well understood by comparing the duration of the quiescent phase and the surface thermal relaxation (or KH) time $t_{\text{KH,surf}}$ defined by Eq. (10). As the surface KH time increases with increasing the stellar mass, the timescale balance changes from $\Delta t_q > t_{\text{KH,surf}}$ to the opposite at some point. Before this, the star contracts significantly during the quiescent phases because the bloated surface layer loses most of its entropy before the next burst begins. After the timescale inversion into $\Delta t_q < t_{\text{KH,surf}}$, the star continues to expand following roughly the mass-radius relation Eq. (9). Here, the same comparison using the global KH time t_{KH} instead of $t_{\text{KH,surf}}$ largely overestimates the critical stellar mass above which the stellar contraction ceases. This is because the global KH time does not consider the inhomogeneous density structure in the stellar interior. Since the mass distribution is very centrally condensed when the star is in the supergiant stage (Figs 5 and 6), the global KH time provides a poor estimate of the thermal relaxation time.

Our calculations show that stellar radiative feedback may become important, if the quiescent phase is longer than $\sim 10^3$ yr. Such long intervals between bursts of accretion are expected for an accretion disk around a growing SMS (Inayoshi & Haiman 2014). If the stellar mass growth is halted by UV feedback, the final mass of the SMS is reduced and the mass of the remnant BH left behind after the star's death is also reduced. Although we have adopted a simple functional form with parameters (Table 1) to model the accretion histories, hydrodynamical simulations will provide more realistic estimates of the final mass. The stellar evolution and strength of the resulting UV radiative feedback will be investigated in future studies.

We thank Kazuyuki Omukai, Kohei Inayoshi and Edward Vorobyov for fruitful discussions. The calculations were in part carried out on PC cluster at Center for Computational Astrophysics, National Astronomical Observatory of Japan. This work is supported in part by Grant-in-Aid for Scientific Research from the JSPS Promotion of Science (25800102, 15H00776, 25287050, and 15J08816). Portions of this research were conducted at the Jet Propulsion Laboratory, California Institute of Technology, operating under a contract with the National Aeronautics and Space Administration (NASA).

REFERENCES

- Agarwal B., Dalla Vecchia C., Johnson J. L., Khochfar S., Paardekooper J.-P., 2014, MNRAS, 443, 648
- Alvarez M. A., Wise J. H., Abel T., 2009, ApJ, 701, L133
- Baraffe I., Chabrier G., Gallardo J., 2009, ApJ, 702, L27
- Becerra F., Greif T. H., Springel V., Hernquist L. E., 2015, MNRAS, 446, 2380
- Bromm V., Loeb A., 2003, ApJ, 596, 34
- Di Matteo T., Khandai N., DeGraf C., Feng Y., Croft R. A. C., Lopez J., Springel V., 2012, ApJ, 745, L29

- Greif T. H., Bromm V., Clark P. C., Glover S. C. O., Smith R. J., Klessen R. S., Yoshida N., Springel V., 2012, *MNRAS*, 424, 399
- Greif T. H., Springel V., White S. D. M., Glover S. C. O., Clark P. C., Smith R. J., Klessen R. S., Bromm V., 2011, *ApJ*, 737, 75
- Hirano S., Hosokawa T., Yoshida N., Umeda H., Omukai K., Chiaki G., Yorke H. W., 2014, *ApJ*, 781, 60
- Hosokawa T., Offner S. S. R., Krumholz M. R., 2011, *ApJ*, 738, 140
- Hosokawa T., Omukai K., 2009, *ApJ*, 691, 823
- Hosokawa T., Omukai K., Yorke H. W., 2012, *ApJ*, 756, 93
- Hosokawa T., Omukai K., Yoshida N., Yorke H. W., 2011, *Science*, 334, 1250
- Hosokawa T., Yorke H. W., Inayoshi K., Omukai K., Yoshida N., 2013, *ApJ*, 778, 178
- Inayoshi K., Haiman Z., 2014, *MNRAS*, 445, 1549
- Inayoshi K., Omukai K., 2012, *MNRAS*, 422, 2539
- Inayoshi K., Omukai K., Tasker E., 2014, *MNRAS*, 445, L109
- Jeon M., Pawlik A. H., Greif T. H., Glover S. C. O., Bromm V., Milosavljević M., Klessen R. S., 2012, *ApJ*, 754, 34
- Kuiper R., Yorke H. W., 2013, *ApJ*, 772, 61
- Latif M. A., Schleicher D. R. G., Schmidt W., Niemeyer J. C., 2013, *MNRAS*, 436, 2989
- Machida M. N., Hosokawa T., 2013, *MNRAS*, 431, 1719
- Madau P., Rees M. J., 2001, *ApJ*, 551, L27
- Marziani P., Sulentic J. W., 2012, *New A Rev.*, 56, 49
- McKee C. F., Tan J. C., 2008, *ApJ*, 681, 771
- Mortlock D. J. et al., 2011, *Nature*, 474, 616
- Omukai K., 2001, *ApJ*, 546, 635
- Omukai K., Palla F., 2003, *ApJ*, 589, 677
- Regan J. A., Johansson P. H., Haehnelt M. G., 2014, *MNRAS*, 439, 1160
- Schleicher D. R. G., Palla F., Ferrara A., Galli D., Latif M., 2013, *A&A*, 558, A59
- Schneider R., Ferrara A., Natarajan P., Omukai K., 2002, *ApJ*, 571, 30
- Smith R. J., Hosokawa T., Omukai K., Glover S. C. O., Klessen R. S., 2012, *MNRAS*, 424, 457
- Stacy A., Greif T. H., Bromm V., 2010, *MNRAS*, 403, 45
- Stahler S. W., Palla F., Salpeter E. E., 1986, *ApJ*, 302, 590
- Van Borm C., Bovino S., Latif M. A., Schleicher D. R. G., Spaans M., Grassi T., 2014, *A&A*, 572, A22
- Visbal E., Haiman Z., Bryan G. L., 2014, *MNRAS*, 445, 1056
- Vorobyov E. I., DeSouza A. L., Basu S., 2013, *ApJ*, 768, 131
- Vorobyov E. I., Zakhochay O. V., Dunham M. M., 2013, *MNRAS*, 433, 3256
- Wu X.-B. et al., 2015, *Nature*, 518, 512
- Yorke H. W., Bodenheimer P., 2008, in *Astronomical Society of the Pacific Conference Series*, Vol. 387, *Massive Star Formation: Observations Confront Theory*, Beuther H., Linz H., Henning T., eds., p. 189
- Yoshida N., Omukai K., Hernquist L., 2008, *Science*, 321, 669